50th AIAA Aerospace Sciences Meeting including the New Horizons Forum and Aerospace Exposition
09 - 12 January 2012, Nashville, Tennessee

AIAA 2012-0872

An Experimental Investigation of the Flow Through the Aft Portion of a High-Flow Nacelle Bypass Concept

Ruben Hortensius[1], Gregory S. Elliott[2], and Michael B. Bragg[3]
University of Illinois at Urbana-Champaign, Urbana, IL, 61801

In order to minimize sonic boom contribution, a conventional turbofan propulsion system was shape tailored to circularize its non-axisymmetric external profile, which, after the addition of a new supersonic inlet and nozzle, has led to a new supersonic propulsion system. A new, secondary, bypass with a highly complex internal geometry was created during this process. The high-flow nacelle bypass geometry includes a forward and aft fairing to direct the flow around the gearbox, a set of thin forward guide vanes, and a set of thick aft guide vanes. The aft guide vanes, which also serve structural purposes, are used to direct the flow such that the exhaust is a uniform, nearly-full annular cross-section, and to choke and then accelerate the flow to supersonic freestream conditions upon exit. A supersonic wind tunnel facility at the University of Illinois was modified and used to simulate the flow through the aft bypass at approximately 6% scale. Two models, one with and one without guide vanes, are studied. Due to facility limitations, the design operating condition could not be achieved; a series of off-design operating conditions are tested instead. Radial pressure surveys are conducted at five azimuthal stations at the inlet to the aft bypass in order to establish in-flow conditions. Static pressure taps on the model surface provide insight into the nature of the flow through the bypass on an individual channel basis. An isentropic-case comparison and mass flow rate calculations were performed. Pressure data were supplemented with surface oil flow visualization and Schlieren imagery. In the off-design conditions tested, results indicate that the channels choke successively, beginning with those that experience the greatest amount of curvature, and hence pressure losses, and ending with those that experience the least curvature, until the entire facility chokes. Also the flow through the aft bypass was found to be highly three-dimensional containing a large amount of flow separation for the conditions tested.

Nomenclature

A	=	local normal area of a channel
A^*	=	area for sonic (M = 1) conditions
A_{throat}	=	minimum (throat) local normal area of a channel
$P_{chamber}$	=	stagnation chamber pressure
M	=	Mach number
M_{tunnel}	=	tunnel Mach number (operating condition)
P	=	generic static pressure
P_0	=	loss corrected stagnation chamber pressure
P/P_t	=	isentropic ideal pressure ratio
PRF	=	total pressure recovery factor
Re_{tunnel}	=	tunnel Reynolds number
R^*	=	normalized radial position
T_0	=	total (stagnation) temperature
θ	=	azimuthal angle
x	=	axial position along the model
x_{cowl}	=	cowling end plane axial position

[1] Graduate Research Assistant, Department of Aerospace Engineering, Student AIAA Member.
[2] Professor of Aerospace Engineering, Associate Fellow AIAA.
[3] Professor of Aerospace Engineering and Executive Associate Dean for Academic Affairs, Fellow AIAA.

Copyright © 2012 by Ruben Hortensius, Gregory S. Elliott, Michael B. Bragg. Published by the American Institute of Aeronautics and Astronautics, Inc., with permission.

I. Introduction

One of the greatest impedances to the common use of supersonic flight is the noise signature created by a sonic boom. Strict FAA guidelines[1] forbid the creation of a sonic boom over populated areas, severely restricting the use of supersonic flight. Low noise signature aircraft, and hence sonic boom attenuation, is therefore an area of research interest.

Sonic boom attenuation may be achieved in many ways. A particular influencing factor is the external shape of the vehicle. Design characteristics such as swept wings, or other morphing technologies, such as Gulfstream Aerospace Corporations' Quiet Spike™, where the nose cone is elongated to morph the forward fuselage into a needle-like shape during high-speed flight,[2,3] have greatly decreased noise characteristics. These types of changes improve upon the noise signature of these aircraft, but the engines and other asymmetric bodies on the airplane also contribute significantly to noise.

Typical turbofan configurations have a gearbox and other protuberances that cause a non-uniform external profile, contributing to sonic boom. Another large source of noise arises from flow spillage from the supersonic inlet. With this knowledge in mind, the Gulfstream Aerospace Corporation proposed a new engine design for use with supersonic business jets (SSBJ) that utilized two key ideas. First, a new supersonic inlet, which yields greatly reduced drag due to spillage at the cost of poor quality flow near the outer wall of the cowling,[5] was used. Second, the external shape of the engine was cylidricalized to remove sonic boom contributions from the nacelle protuberances by wrapping the entire structure with a secondary cowling. A new, secondary bypass duct, not to be confused with the turbofan bypass, is created upon addition of the cowling. A new aft plug nozzle completes the proposed design, as illustrated in Fig. 1. The proposed Rolls-Royce Tay turbofan core engine has a maximum takeoff thrust of about 15,000 lbf and a bypass ratio of about 3 (Fig. 2).

Just aft of the inlet, a splitter plate separates the flow streams entering the turbofan from those which enter the bypass. The poor quality flow near the outer wall passes on the outside of the splitter plate and enters the bypass duct, instead of entering the core turbofan. In this manner, the overall sonic boom is greatly weakened since the contribution due to spillage and that due to nacelle protuberances are both reduced. However, the excessive internal blockage, due to the highly complex flow path within the bypass duct, was found to couple strongly with inlet performance as the normal shock moved upstream.[6] Therefore, a clear understanding of the flow within the bypass duct is of great importance to the efficiency of the entire SSBJ engine concept.

The bypass has an annular cross section at its inlet and, as the turbofan protuberances and gearbox are approached, a fairing diverts the flow such that the cross section becomes a partial annulus. Nine thin, plate-like vanes guide the flow as it is contracted by a forward fairing. At its maximum, the fairing encompasses 160° (44.4%)

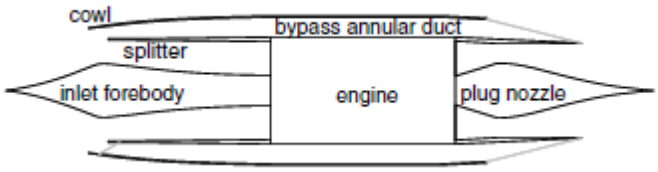

Figure 1. High flow nacelle bypass engine concept.

Figure 2. Rolls-Royce Tay-type turbofan.

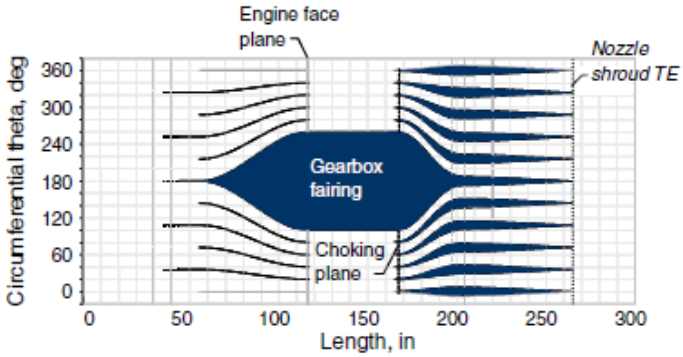

Figure 3. Unwrapped bypass duct geometry.

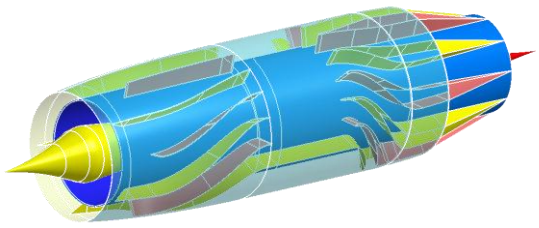

Figure 4. CAD representation of the complete engine concept.

of the annulus. Once past the turbofan protuberances, the fairing closes and terminates at the bypass exhaust. Nine other relatively thick guide vanes, intended to reaccelerate the flow to supersonic freestream conditions, are located in the aft portion of the bypass duct as the fairing shrinks and closes.

Figure 3 shows an unwrapped schematic of the bypass geometry laid on the full engine geometry platform. Flow is from left to right. The gearbox fairing is centered about the bottom-center (azimuthal angle, θ, of 180°). The forward vanes, which have constant contraction ratios, end when the fairing has reached its maximal size, that is, within the fully blocked region, which coincides with the core engine inlet plane. The aft vanes begin at the onset of the gearbox closing fairing and extend to the nozzle shroud trailing edge. Upon exiting the cowling, the aft vanes decrease in height linearly to their point of termination at the core engine trailing edge. A three dimensional CAD model of the full engine configuration is shown in Fig. 4 wherein the supersonic inlet cone, forward bypass vanes, gearbox fairing, and aft bypass vanes are clearly visible.

In a study conducted by Yeong[7,8] at the University of Illinois, an axisymmetric wind tunnel was designed and built at approximately $1/6^{th}$ scale to study the first generation bypass model design. A concurrent study, conducted by Chiles,[9,10] completed a CFD comparison to the experimental results. Both studies found that the gearbox blockage contributed greatly to increased pressure losses, especially as there was heavy flow separation at the fairing closing. Chiles also concluded that the forward fairing geometry was effective at diverting the flow around the gearbox.

Later designs incorporated updated geometry and different design operating conditions. As a result, subsequent experimental efforts conducted on the updated geometry were broken into forward and aft segments where each utilized a separate facility. Further forward bypass experiments were carried out by Hererra.[11]

Kim, Kumano, Liou, Povinelli, and Conners[6] conducted a CFD simulation of the full engine including the bypass duct with fore and aft fans. In this study, boundary conditions at the core turbofan inlet and exit were applied from an embedded solver to reflect the core engine performance characteristics. They found that the flow through the highly complex bypass duct greatly influenced the performance of the supersonic inlet. The original design vane geometry used in Ref. 6 is the same that which is used in the present study. In a second study, Kim, Kumano, Liou, and Povinelli[12] explored the optimization of the aft vane geometry to achieve design specifications. A comprehensive summary of the high-flow bypass concept, its feasibility, and research to-date is provided by Conners and Wayman.[13]

This study is an investigation of the flow through the aft bypass. The purpose is to provide an experimental 'proof-of-concept' of the overall configuration. Specifically, the flow quality at the aft bypass inlet plane, located within the aft section of the fully blocked region, is assessed. Flow within the aft channels is then assessed by means of various pressure data, a mass flow rate analysis, and an isentropic comparison. Additional supplementary data is provided by means of surface oil flow visualization and Schlieren photography. Due to facility limitations, design operating conditions could not be achieved; a series of off-design operating conditions are tested instead.

II. Experimental Methods

Since this study regards the aft bypass geometry and flowfield, the experimental setup was unconcerned with the details of the engine geometry prior to the fully blocked region. This allowed for a simplified wind tunnel design, especially when compared to the facility used to evaluate the forward bypass region as conducted by Yeong,[7,8] and thereafter, Herrera,[11] where a cantilevered, axisymmetric, centerbody with inlet cone is mounted within a tubular wind tunnel. In this instance, the full gearbox blockage was extended upstream into the stagnation chamber.

A. Wind Tunnel Description

An existing supersonic wind tunnel originally constructed for axisymmetric base-flow experiments by Sauter[14] was very well suited for this investigation and so was modified and used for the duration of this study. The full aft bypass facility is illustrated in a partial cross-sectional view in Fig. 5. The wind tunnel, located at the University of Illinois, is a blowdown-type facility with an annular cross section and a 4.00 inch throat diameter. A central sting, supported within the stagnation chamber and secured with a taper lock at the back of the chamber, extends along the tunnel centerline through the flow conditioners and nozzle, and ends just inside of the viewing chamber. The viewing chamber has several windows to allow for optical diagnostic techniques such as Schlieren photography, surface oil flow visualization, or laser-based techniques.

Air is supplied from a tank farm which is filled by two compressors. The air supply pipe enters the facility building, and, after passing through a manual gate valve for redundancy and then a FlowServe valve, enters the schedule 40 pipe cross stagnation chamber from above through a 6 inch pipe. The flow is directed towards the back of the chamber to encourage uniform stagnation conditions within the chamber. The maximum stagnation pressure

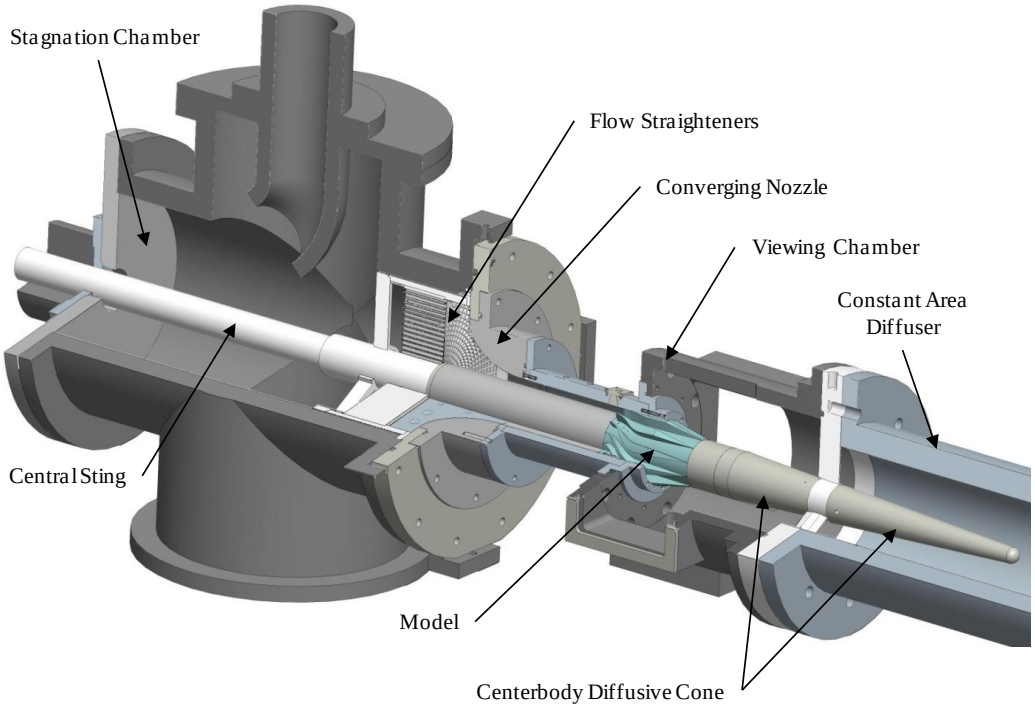

Figure 5. Partial cutaway view of the full aft bypass facility with clean model installed.

required for this study was only about 22 psia, while it was originally designed for operating pressures three times greater than that. Total temperature, T_0, is monitored within the chamber and a pressure transducer monitors chamber pressure, $P_{chamber}$.

The overarching concept behind the aft bypass facility design was to extend the full gearbox blockage as far upstream as possible. An assembly simulating the inner bypass surface and the gearbox blockage was designed to slide over the central sting. This assembly was projected upstream into the converging nozzle and up to the flow conditioners. Aft of the model, which was also designed to slide over the sting, the centerbody was extended in the downstream direction and ultimately terminated in a diffusive cone. The two part diffusive cone was supported by a three-spoked flange fastened to the viewing chamber's downstream face.

Within the converging nozzle, two plates, projecting radially from the centerbody and fitting into slots within the nozzle to properly separate the blocked and unblocked regions, represented the gearbox blockage radial surfaces. A partial annular flange was positioned underneath of these plates, directly downstream of the flow conditioners, to fully close all flowpaths through the gearbox and isolate the blocked region.

The nozzle throat diameter of 4.00 inches dictated the geometric scaling of the experimental setup as defined by the full scale engine, yielding a 6% scale. A constant area component was used to represent the outer bypass wall, or cowling. The model is positioned axially to line up appropriately with the cowling end plane as the design specifies, thereby allowing the model to exhaust into the much larger-diameter viewing chamber. The first segment of the diffusive cone is a cylindrical cap in which the pressure lines leaving the models can be turned around in and allowed to exit the facility through the hollow central sting. The second part is a two-part diffuser with a 3° half angle.

B. Experimental Models

Two aft bypass models were used in this study. The first, known as the clean model, is devoid of the aft guide vanes and consists of the inner bypass surface and the gearbox fairing. It was used as a baseline model. The second model, known as the vaned model, also includes the aft guide vanes. The models, which are of SLA construction, are 6.12 inches long. The fully blocked region persists for the first 0.28 inches along the models, which is where the gearbox fairing curvature begins and vane forward tips are located.

Model surface static pressure taps have a diameter of 0.045 inches. Inside the model, the internal pressure lines turn in the downstream direction with a bending radius of 0.045 inches, at which point they continue down the length the model to exit on the model end face. A minimum separation distance of 0.050 inches was enforced between any two internal pressure lines. 0.5 inch deep, 0.067 inch diameter counterbores allow for the insertion of

lengths of stainless steel tubing, which are connected to pressure transducers via nylon pressure tubes. The end face of the model is located approximately 0.75 inches from the end of the central sting. The stainless steel tubing protruding from the model internal pressure line counterbores were then bent such that they faced upstream through the central sting. In this manner, the model surface static pressure readings exited the facility through the central sting.

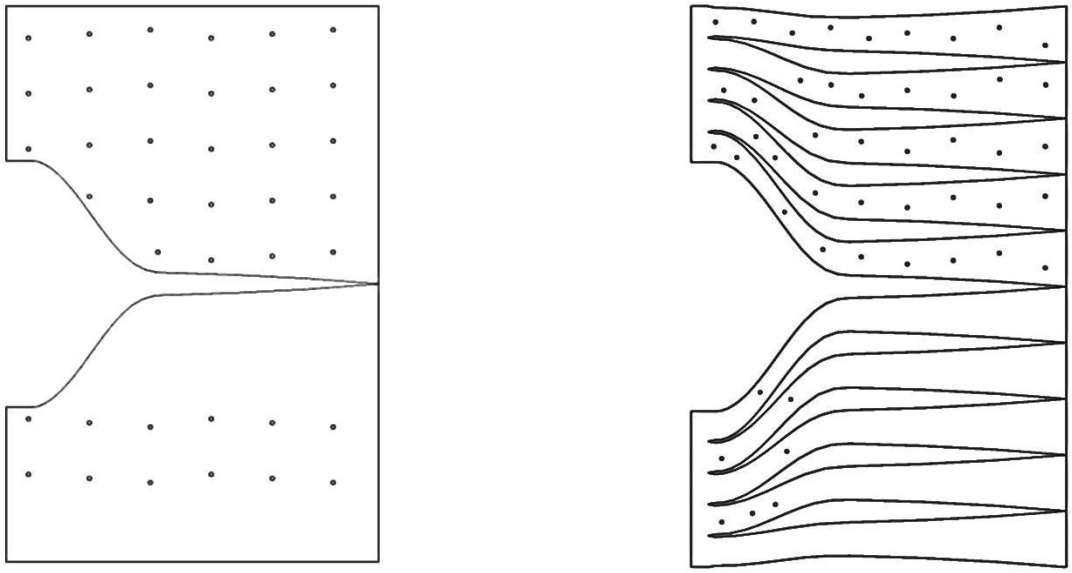

a) b)

Figure 6. Location of model surface static pressure taps on the unwrapped a) clean, b) vaned model.

1. Clean Model

The clean model has thirty-nine model surface static pressure taps arranged in seven rows. Five rows are located on one side of the model, known as the primary side. The other two rows are located on the opposite side, known as the complementary side, and are located exactly symmetrically of two primary rows so as to allow for flow symmetry checks. The clean model surface static pressure tap rows are located at azimuthal positions corresponding to the centerline of the aft guide vane exits. Figure 6 a) shows the locations of the clean model surface static pressure taps on the unwrapped geometry.

2. Vaned Model

Forty-nine taps, most located on the primary side of the vaned model, were arranged near the centerlines of the channels. Due to space constraints, some taps had to be placed on the other side of the model. Figure 6 b) shows the locations of the vaned model surface static pressure taps on the unwrapped geometry.

A naming convention for the vanes and channels of the bypass as established in Ref. 6 is used. As shown in Fig. 7, channels are numbered 1-5 by increasing curvature so that Ch $^{\#}1$ is near the top of the annulus where the flow path is relatively straight, whereas Ch $^{\#}5$ is directly adjacent to the highly curved gearbox fairing such that it comprises one wall of the channel. Since the model is symmetric, only five channels need be identified. The compliment (symmetric) channels follow the same naming scheme, but are distinguished from the primary side by the subscript 's'. Additionally, the azimuthal angle, θ, is measured from the top-center location. Positive θ is assigned to the primary side of the model, whereas negative θ is on the complementary side. Also shown in the figure, is each channel's azimuthal centerline angle.

C. Facility Operating Condition Definition

A LabVIEW code was written to collect and process pressure data. The wind tunnel was manually operated using the gate valve. The primary metric to ensure constant wind tunnel operating conditions was the pressure ratio between a single, model invariant, static tap, P_{stOP}, at the inlet plane and the stagnation chamber pressure, $P_{chamber}$. A pressure recovery factor, *PRF*, was determined for each operating condition by calculating the ratio of the core flow probe total pressure at a single azimuthal station to the stagnation chamber. It was used to accurately estimate local total pressure at the inlet plane, regardless of whether or not the probe was in the wind tunnel. In this manner, the

stagnation chamber pressure for a specific operating condition was corrected for losses, such that the corrected total pressure, P_0, is defined as

$$P_0 = P_{chamber} \cdot PRF \tag{1}$$

In order to accurately define the true operating condition, the tunnel Mach number, M_{tunnel}, was defined and it is the metric used to designate tested operating conditions. M_{tunnel} is the isentropic Mach number for the loss corrected total pressure and is defined as

$$M_{tunnel} = \sqrt{\frac{2}{\gamma - 1} \cdot \left[\left(\frac{P_{stOP}}{P_0} \right)^{\frac{1-\gamma}{\gamma}} - 1 \right]} \tag{2}$$

Model surface static pressure tap data were normalized by P_0 to allow for comparison between data sets and operating conditions. Inlet plane data did not use such a correction since the total pressure probe measured the true local total pressure.

D. Pressure Data

1. Inlet Plane

In order to evaluate flow conditions entering the aft bypass model, pressure data were taken at a plane within the full blocked region located approximately 1.4 inches upstream of the start of the gearbox fairing curvature and vane upstream tips. A total pressure probe was traversed in the radial direction at five azimuthal stations. The azimuthal stations were positioned to coincide with the center of each of the channel inlets, as indicated in Fig. 7. An outer bypass wall static pressure tap was also located at each azimuthal station. The total pressure probe, acquired from United Sensor Corporation, had a 0.049 inch diameter, a chamfered tip and a 90° miter joint. Boundary-layer (as by probe total pressure) and Mach (assuming constant radial static pressure) profiles were generated from these data sources. Five total pressure probe traverses were conducted at each azimuthal station for a given operating condition.

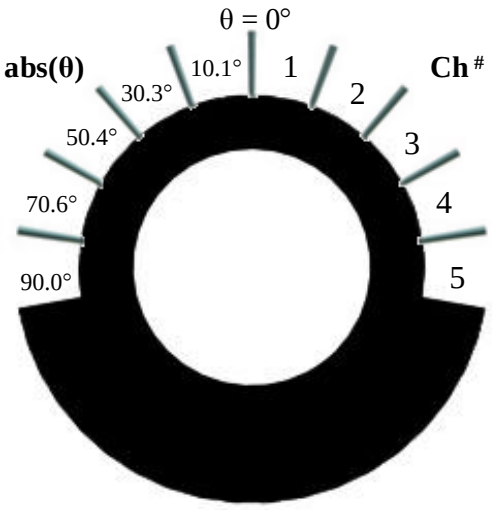

Figure 7. Convention for channel naming. The azimuthal angle (θ) for each channel's centerline at the aft vane forward tips is also given.

2. Model Surface Static Pressure Taps

Pressure data from the model surface static pressure taps were only collected for runs where the total pressure probe was not present in the flow. At least five runs were conducted and, after checking for data consistency, the results were averaged to produce one representative run for each operating condition. Model pressure data were normalized by P_0 to allow for comparison between runs, however, it is important to recognize that P_0 is not necessarily a good representation of total pressure everywhere within the facility.

E. Flow Visualization Techniques

1. Schlieren Photography

A conventional, z-type Schlieren system was used to capture images of the flow exiting the bypass region. Through the use of both horizontal and vertical knife edges, changes in the index of refraction due to flow density gradients in the vertical and horizontal directions, respectively, were visualized. The point LED source was used in pulse mode to provide instantaneous images (20 μs), of which approximately 250 were collected for each run condition using a charge coupled device (CCD) camera and lens. Imagery for low M_{tunnel} cases were not expected to yield very distinct images since the density gradients for these subsonic flows were quite small.

2. Surface Oil Flow Visualization

Surface oil flow visualization was conducted using two slightly different methods during the course of this study. First, a mixture consisting of motor oil, kerosene, and an artist's pigment called lampblack, was applied to the model surface using a paint brush. The tunnel was allowed to run, and while surface shear stresses from the fluid caused it

to move, the mixture, due to volatile characteristics of kerosene, dried. The results were recorded with a digital camera.

The second, more detailed, surface oil flow visualization was conducted on both the clean and vaned models. This time, a 1/8th inch grid was drawn on black contact paper, which was then cut from stencils and carefully applied to the model. Using a hypodermic syringe with a 26.5 gauge needle, minute amounts of a new mixture were applied on the grid points. This mixture consisted of STP oil treatment and a few drops of a liquid fluorescent dye. SAE 10W-30 motor oil was added in order to decrease the mixture viscosity for any low Mach number operating conditions. Figure 8 depicts the prepared clean model prior to insertion into the wind tunnel. Still images were recorded under ultraviolet light.

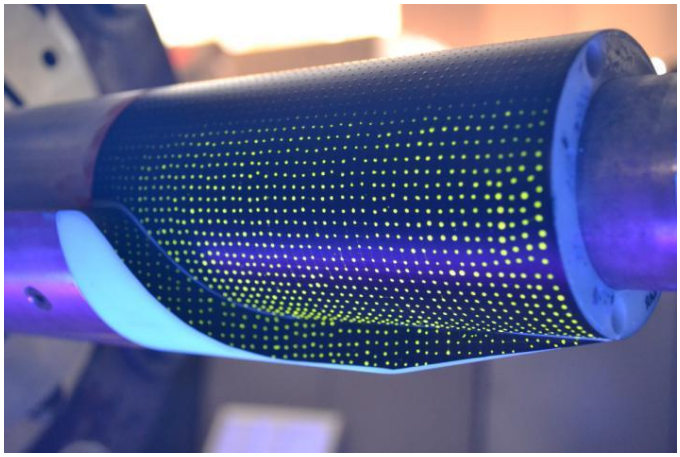

Figure 8. The fully prepared clean model for fluorescent surface oil flow visualization.

III. Results and Discussion

The prescribed inlet plane Mach number that this study intended to achieve (M_{tunnel} = 0.700) was easily achieved with the clean model. However, when the vaned model was installed in the wind tunnel, the facility choked prior to achieving the design point. The vaned model test maximum achievable tunnel Mach number was 0.538. While clean model data were only collected at a single operating condition, data were collected at several operating conditions for the vaned model. Two choked flow operating conditions were run for the vaned model. They were distinguished from each other by their respective subscripts which indicate the approximate P_0. Table 1 presents the test matrix employed in this study, the results of which are subsequently presented.

In order to conduct a survey of the inlet plane, the wind tunnel needed to run at a relatively constant operating condition while the probe traversed radially. This took approximately 80 seconds to complete. The variation in operating condition during a run was assessed by calculating the average percent change in $P_{chamber}$, M_{tunnel}, and the tunnel operating Reynolds number, Re_{tunnel}, during the course of a traversing run as shown in Table 2. Results show that for the lowest operating conditions variations exceeded the maximum allowable goal of 5%. This is likely due to the fact that the valves used to control stagnation chamber pressure provide the most control within the mid-range, that is, half way open. Variations for the other operating conditions proved to lie well within the desired allowable range.

Table 1. Aft Bypass Experimental Study Test Matrix

M_{tunnel}	Test Model	Inlet Plane Survey	Model Surface Static Taps	Schlieren		Surface Oil Flow	
				Horiz.	Vert.	Lampblack	Fluorescent
0.148	Vaned	x	x	x	x		x
0.294	Vaned	x	x	x	x		
0.385	Vaned	x	x	x	x		x
0.481	Vaned	x	x	x	x		
0.531	Vaned	x	x	x	x		
$0.538\|_{20.00}$	Vaned	x	x	x	x		
$0.538\|_{21.00}$	Vaned	x	x	x	x		x
0.704	Clean	x	x	x	x	x	

Table 2. Average Percentage Variation of Facility Operating Condition

OP: M_{tunnel}	Test Model	$P_{chamber}$ (psia)		M_{tunnel}		Re_{tunnel}	
		Mean	%Δ	Mean	%Δ	Mean	%Δ
0.148	Vaned	14.676	0.19	0.148	5.96	45743	6.32
0.294	Vaned	15.274	0.29	0.294	2.42	95452	2.18
0.385	Vaned	16.370	0.52	0.383	1.95	132646	1.70
0.481	Vaned	17.655	0.73	0.480	1.41	169296	1.85
0.531	Vaned	18.937	0.99	0.526	0.93	198404	1.74
$0.538\|_{20.00}$	Vaned	19.998	1.10	0.537	0.44	213710	1.49
$0.538\|_{21.00}$	Vaned	21.002	1.19	0.537	0.38	223582	1.60
0.704	Clean	19.405	0.64	0.701	1.14	244531	1.33

A. Inlet Plane Data

A total pressure survey was conducted at the inlet plane for all tested operating conditions. The probe was traversed at five azimuthal stations located at the center of each channel. Total pressure within the core flow (removed from the boundary layers) was very uniform, as summarized in Table 3, where the maximum coefficient of variance (CV) at any location was less than 0.20%. Conditions across azimuthal stations were also extremely uniform; the maximum core flow P_{total} CV was measured for the M_{tunnel} = 0.531 operating condition and was still only 0.36%.

Boundary layers on both the inner and outer walls were assessed. Apart from at the Ch #5 azimuthal location, both inner and outer wall boundary layers exhibited very uniform characteristics and showed no correlation between boundary-layer thickness and azimuthal location or operating condition. Inner wall boundary layers were observed to be thicker than those of the inner wall (up to 70% thicker), most likely due to the fact that the inner wall boundary layer had a longer distance over which to grow. At the Ch #5 azimuthal location (near the gearbox), boundary layer thicknesses and velocity and momentum deficits were found to be much increased. This was largely attributed to wall effects.

An outer wall static pressure tap was placed just upstream of total pressure probe tip to allow for the calculation of Mach number and velocity. Unfortunately, the static pressure taps were located too close to the total pressure probe tip and so the readings were influenced by the probe's presence. In order to remedy this problem, an empty tunnel run (without a probe) was also conducted to provide a representative static pressure. Under a constant pressure ratio constraint, the representative static pressure was then adjusted to account for any small differences in P_0 between the two runs. In all subsequent total pressure probe profiles, the adjusted (representative empty tunnel) static pressure was used for calculations.

Mach number radial profiles for several operating conditions are found in Fig. 9. When plotting radial profiles, the normalized radial position, R^*, is used such that R^* is equal to zero at the inner wall and is unity at the outer wall. Due to the probe's finite diameter, the traversing sequence typically does not reach $R^* = 0$ or 1.

Table 3. Summary of Inlet Plane Total Pressures (psia)

M_{tunnel}	Ch #1		Ch #2		Ch #3		Ch #4		Ch #5	
	Mean	%CV	Mean	%CV	Mean	%CV	Mean	%CV	Mean	%CV
0.148	14.652	0.005	14.673	0.006	14.669	0.008	14.673	0.007	14.662	0.009
0.294	15.258	0.014	15.259	0.030	15.257	0.009	15.258	0.036	15.234	0.010
0.385	16.315	0.020	16.301	0.041	16.391	0.044	16.298	0.074	16.356	0.038
0.481	17.589	0.057	17.609	0.065	17.574	0.065	17.617	0.041	17.626	0.085
0.531	18.862	0.070	18.909	0.140	18.825	0.181	18.951	0.089	18.769	0.128
$0.538\|_{20.00}$	19.928	0.040	19.953	0.072	19.945	0.045	19.953	0.096	19.914	0.103
$0.538\|_{21.00}$	20.953	0.112	20.942	0.094	20.947	0.137	20.933	0.097	20.944	0.126

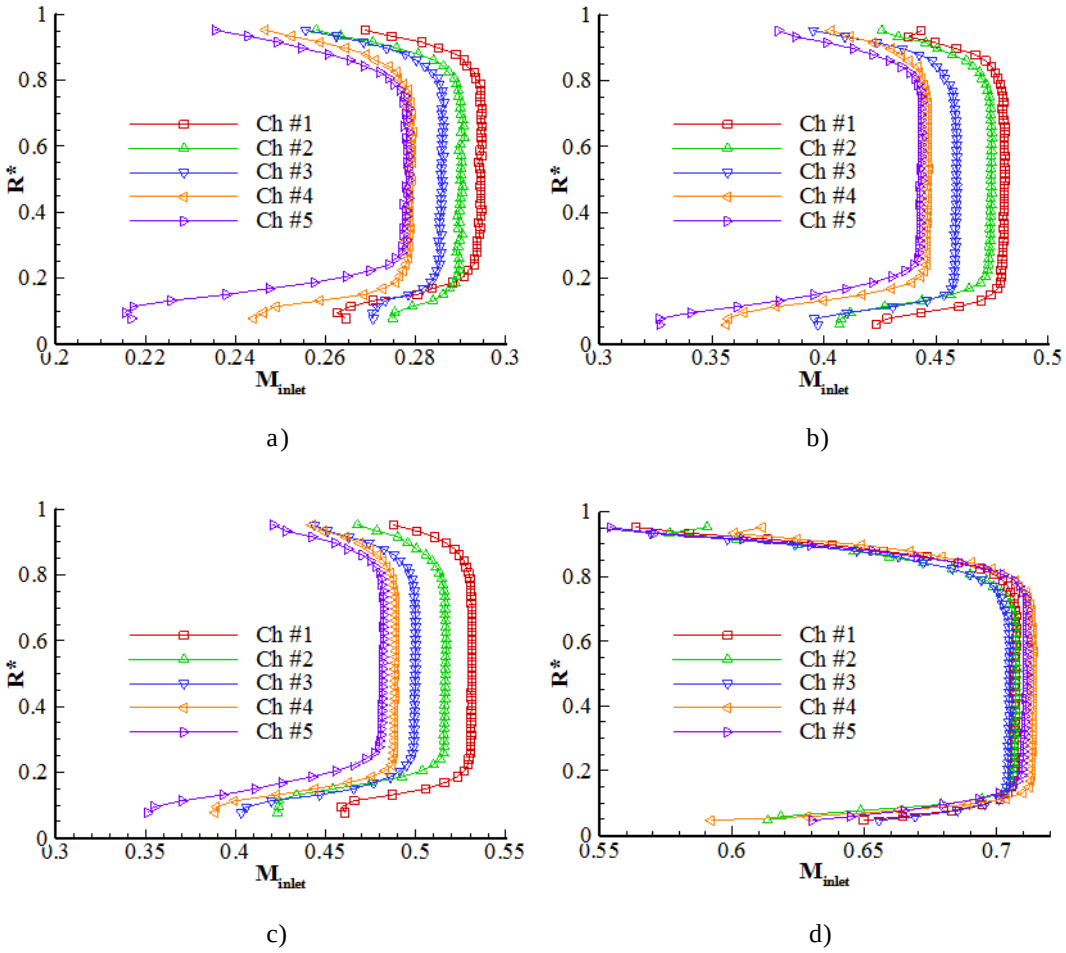

Figure 9. Radial Mach profiles at the inlet plane at each channel inlet for a) vaned model at M_{tunnel} = 0.294, b) vaned model at M_{tunnel} = 0.481, c) vaned model at M_{tunnel} = 0.531, and d) clean model at M_{tunnel} = 0.704.

For the clean model operating condition (M_{tunnel} = 0.704, shown in Fig. 9 d), the flow Mach number at the azimuthal stations nearest the gearbox walls (Ch #4 and Ch #5) is slightly higher than that nearer the top of the annulus. This is in contrast to the vaned model (Fig. 9 a - c). For these cases, the flow Mach number decreases as θ increases so that the highest recorded core Mach number for a given operating condition is located at the inlet to Ch #1, and the lowest channel inlet Mach number is recorded for the channel adjacent to the gearbox fairing: Ch #5. This trend is evident for all tunnel operating conditions and no obvious difference exists between the choked and un-choked cases. It is important to note that $\theta_{Ch^{\#}5}$ and $\theta_{Ch^{\#}1}$ are 10° removed from the gearbox fairing and top-center location, respectively. Subsequently, no quantitative statements can be said about the flow Mach number any nearer to the fairing or nearer to top-center. Due to wall effects, the total amount of azimuthal variation in the core flow Mach number is likely greater than was measured.

The relationship between M_{inlet} and $|\Theta|$ could be interpreted to indicate that the channels with less curvature have a tendency to pass more relative mass than the channels nearer to the gearbox fairing since M_{inlet} is greater near top-center. A possible theory is that as the total mass flow increases (and M_{tunnel} with it), the total pressure losses within the channels that undergo a greater degree of curvature increase until the losses become too great, and they can no longer pass the needed mass flow. To compensate, the channels undergoing less curvature (and less pressure losses) would be forced to pass the additional mass flow. In this manner, pressure losses due to channel geometry would limit mass flow rates (causing choked conditions), lead to dumping, and ultimately to increased M_{inlet} near the top-center location. This successive choking or mass flow dumping theory may also contribute to the observed differences in the inlet plane boundary layer characteristics near the gearbox.

B. Surface Static Pressure

1. *Clean Model*

A sufficient amount of model surface static pressure data were collected to check that the readings were consistent. Flow symmetry checks were carried out using the two complementary rows of taps placed on the clean model. The results indicated fairly good symmetry.

In general, the pressure ratios increase with downstream location along each row of static pressure taps on the clean model. This indicates that the flow Mach number is decreasing. It is difficult to quantify this decrease because the data normalization is carried out by P_0, a value that is not necessarily representative of the local total pressure at all locations on the model, particularly in regions of flow separation. However, since total pressure cannot increase, it can be safely said that the Mach number over the model does in fact decrease, even if the decrease cannot be quantitatively be assessed.

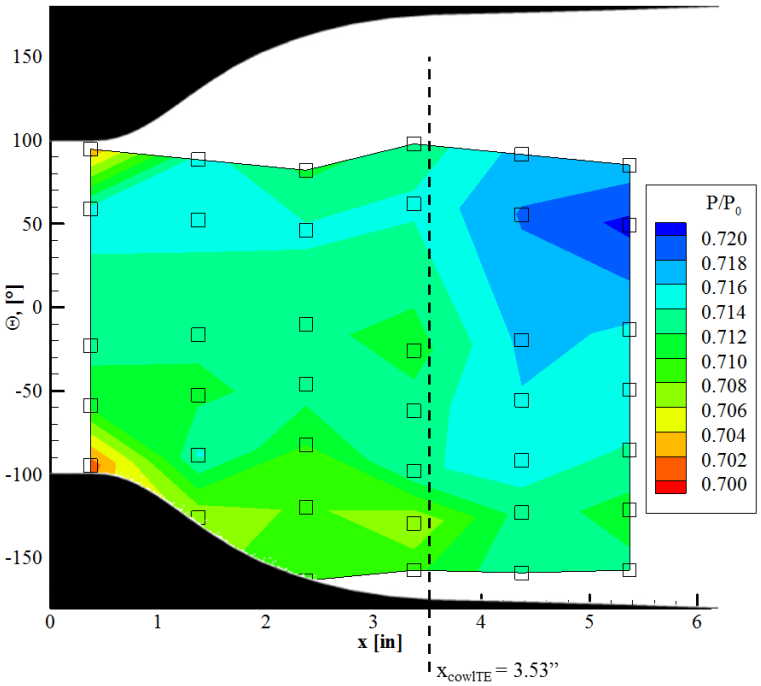

Figure 10. Clean model surface static pressure contour plot for M_{tunnel} = 0.704.

Clean model data were displayed in a contour plot of the unwrapped model surface (Fig. 10) where the normalized static pressure is plotted. At the first axial data plane, two lower pressure ratio regions exist near each of the fairings. Between the low pressure regions exists a region of higher pressure near the top of the annulus (small θ). As the flow progresses downstream, the pressure ratio increases, especially when the flow exits the cowling (x = 3.525 in).

2. *Vaned Model Channel Data*

Vaned model data were analyzed on an individual channel basis. The static pressures recorded within each channel were normalized by that channel's core total pressure as measured at the inlet plane. In an effort to provide added insight into the internal flows within the aft bypass channels, composite images of the flattened inner surface of each channel under fluorescent surface oil flow visualization were generated for the $M_{tunnel} = 0.538|_{21.00}$ operating condition and presented with the pressure data. The locations of static pressure taps are superimposed on the images.

The normalized pressures for each channel were plotted, for each operating condition, versus model axial position, x. The local normal channel area, A, is plotted on the secondary axis as normalized by that particular channel's minimum (throat) area, A_{throat}. Figures 11-15 display the channel pressure data in order of increasing channel number.

Regardless of axial position, the pressure ratio decreases as M_{tunnel} increases, as would be expected by the isentropic relations. Another expected result is that for all stations beyond x_{cowl}, the pressure ratio remains constant, regardless of channel number, confirming that the desired experimental setup was achieved; all channel flows encounter the same farfield conditions upon exiting the cowling, bringing them to uniform static pressure. For instance, for the M_{tunnel} = 0.531 case, the mean pressure ratio for all model surface static pressure taps beyond x_{cowl} is 0.744 with a CV of 0.13%. Among all operating conditions, the largest CV is 0.14%, showing great consistency in the data.

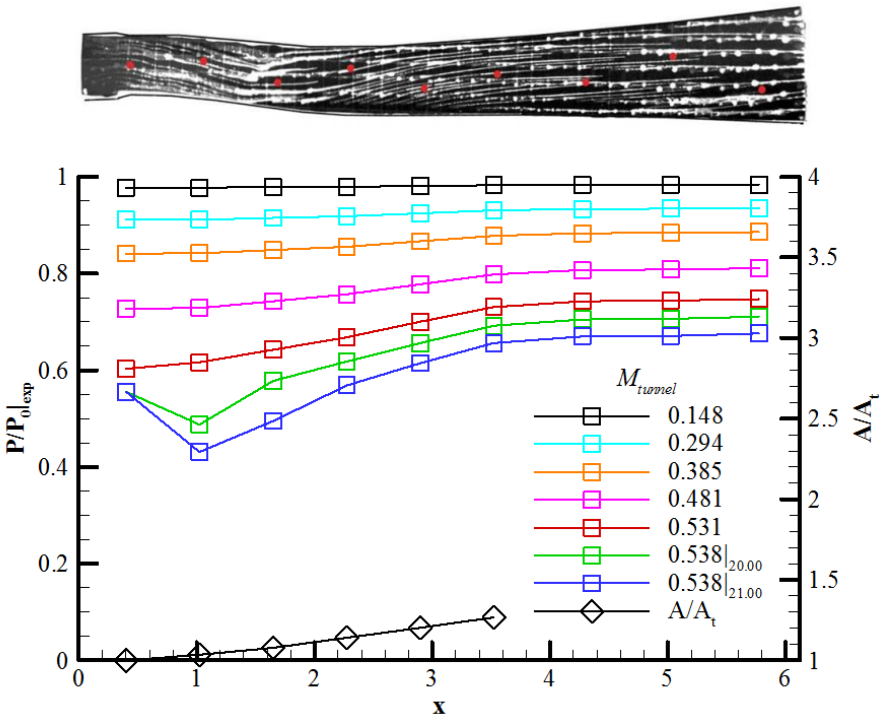

Figure 11. Normalized experimental pressure ration within Ch #1 for all tested operating conditions.

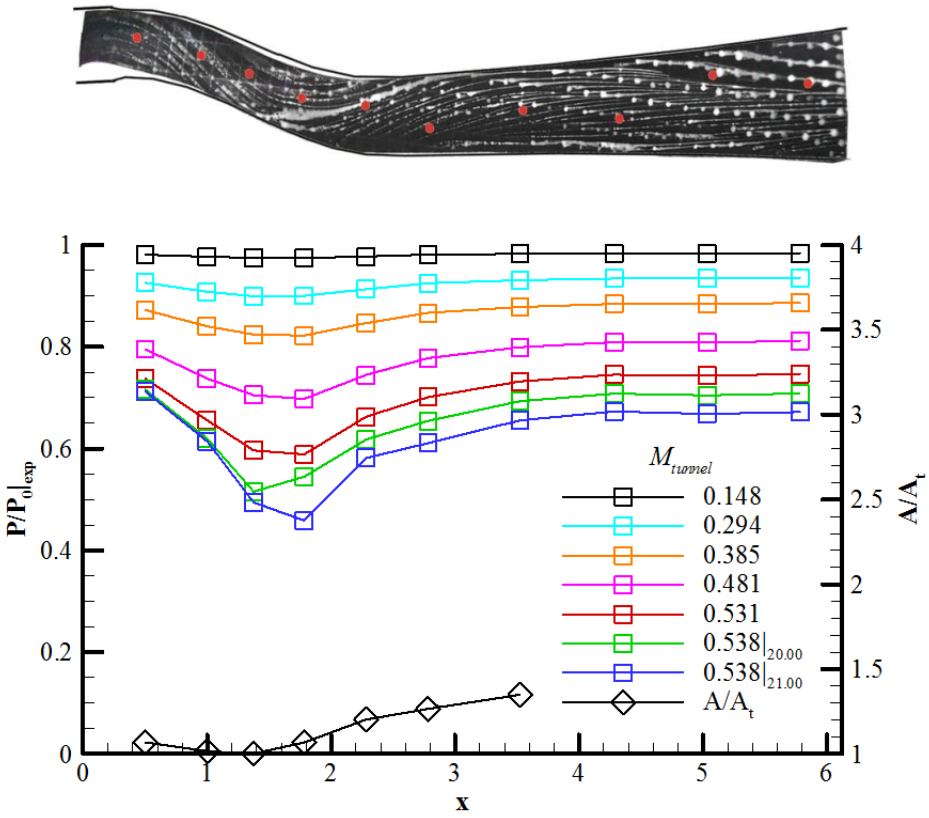

Figure 12. Normalized experimental pressure ration within Ch #2 for all tested operating conditions.

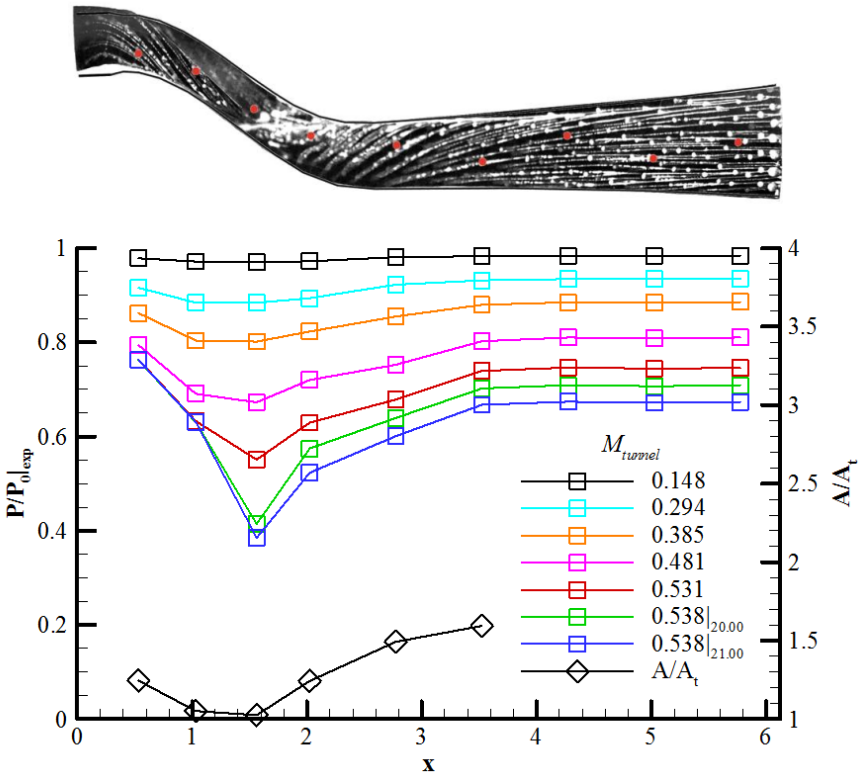

Figure 13. Normalized experimental pressure ration within Ch #3 for all tested operating conditions.

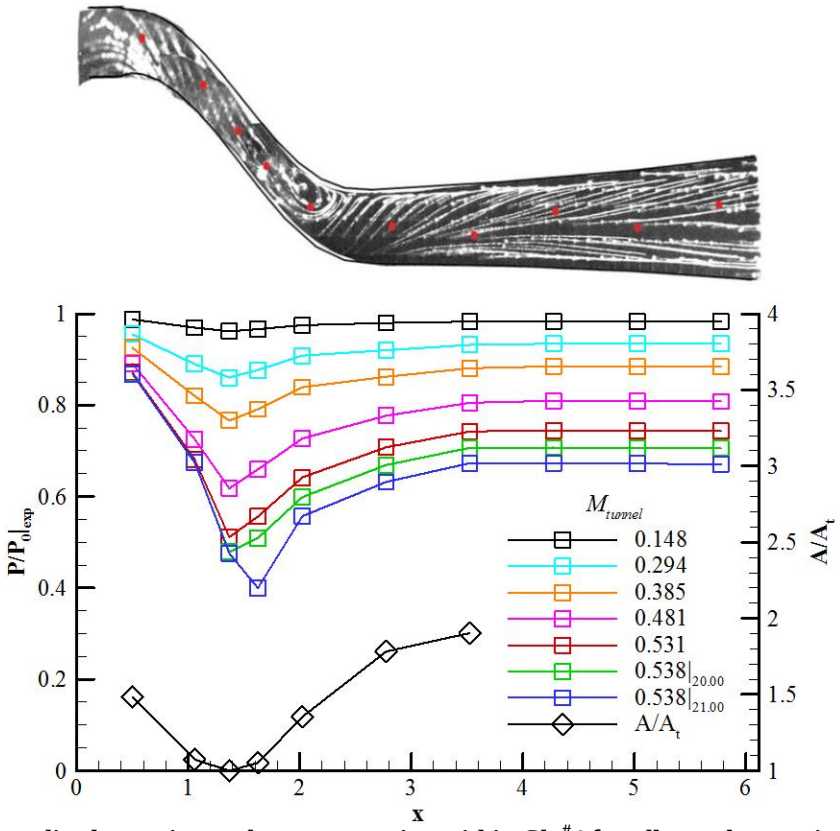

Figure 14. Normalized experimental pressure ration within Ch #4 for all tested operating conditions.

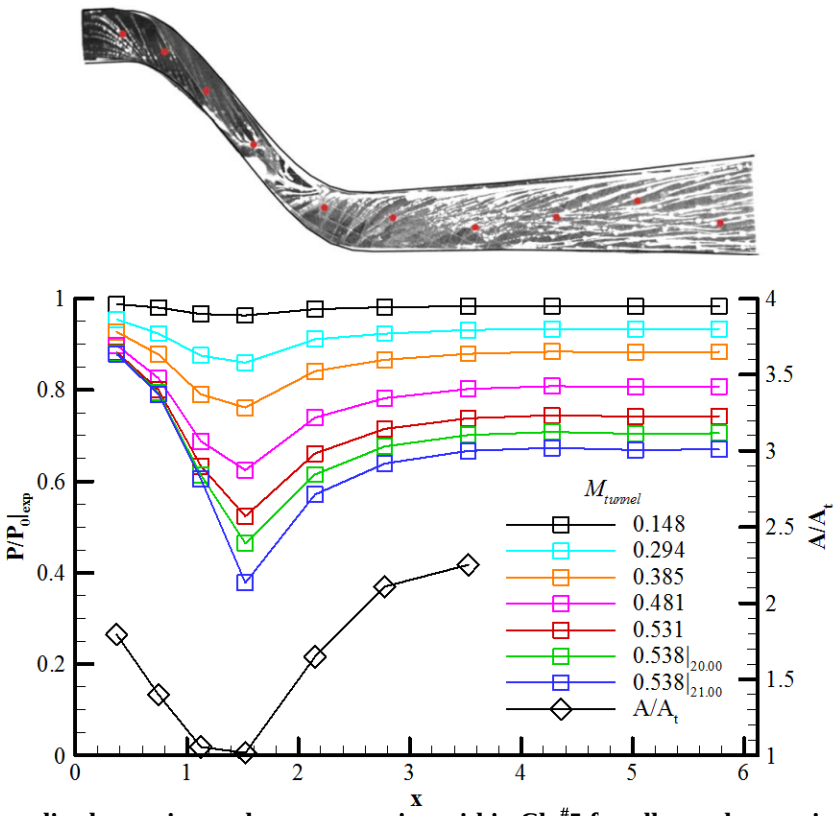

Figure 15. Normalized experimental pressure ration within Ch #5 for all tested operating conditions.

The shapes of the pressure ratio curves found in the data are representative of the curves typically found in a converging diverging nozzle. As the area ratio decreases within the converging section, the flow accelerates, and the channel pressure ratio decreases. Beyond the channel throat, the curves can take multiple routes, depending on flow conditions. In the lower limit, supersonic conditions are not achieved at any location within the channel, and the curve takes a subsonic route, where the pressure ratio returns to unity as the flow slows in the diverging section. In the high limit, supersonic conditions are achieved everywhere, and the pressure ratio reaches the sonic limit at the throat, and then continues to decrease as the supersonic flow accelerates through the diverging section. In the last case, which occurs for the choked operating conditions in this study, supersonic conditions are achieved at the throat, but a shockwave within the diverging section causes the flow to return to subsonic conditions.

Experimental pressure ratios clearly fall below the sonic condition (P/P_0 = 0.528) for at least two data series (the choked operating conditions) in every channel. Total pressure losses would tend to increase the pressure ratio (to possibly above the sonic limit), but at the lowest observed pressure ratio, a total pressure loss of more than 24% would be required to return to sonic conditions. Such a large degree of total pressure losses over such a short distance would be highly unlikely. When coupled with the observation that the minimum observed pressure ratio usually occurs at some point downstream of the channel throat, it becomes clear that the flow must achieve supersonic conditions, but that shock structures must be responsible for a return to characteristically subsonic pressure ratios further downstream.

Since any pressure jump across a shockwave would be a localized effect, and, perhaps more importantly, its location would most likely fluctuate greatly, capturing the pressure discontinuity in the data would be impossible given the limited number of pressure taps within each channel. No obvious evidence of shock presence was found in the surface oil flow visualizations.

Limitations in the experimental setup limited the operating conditions to less than what was desired (since fully supersonic flow conditions were not achieved). However, off-design aft bypass performance data is still highly valuable towards the understanding of the characteristics of the flow through this highly complex geometry.

The surface oil flow visualization composite images indicate, by the increasing prevalence of a recirculation region near the channel throat, that flow complexity increases greatly with channel number; a not unexpected result. Since a larger degree of flow reversal and complexity is nearly always associated with greater total pressure losses,

it is very likely that Ch #1 undergoes the least amount of pressure losses and that Ch #5 experiences the most. This observation fits well with the proposed mass dumping theory.

The channel pressure data also supports the successive choking theory. As channel number increases, more and more operating conditions share the same pressure ratio at the first channel static pressure tap. For instance, only the two choked operating conditions share the same pressure ratio at the first tap within Ch #1 (Fig. 11), but, within Ch #5 (Fig. 15), four operating conditions share the same ratio. Since four operating conditions share the same experimental pressure ratio at the first tap within Ch #5, it must choke before the entire facility chokes. Once the last channel chokes (Ch #1), the entire facility chokes.

3. *Isentropic Channel Comparison*

A comparison between experimental conditions and isentropic calculations was conducted. For the purposes of this computation, it was assumed that total pressure was conserved from the inlet plane to the location of the first model surface static pressure tap within each channel. As before, it was further assumed that the wall static pressure was representative of conditions within the core flow of the channel. Total and static pressure conditions at the first channel static tap were used to determine the Mach number, from which the isentropic area ratio, A/A^*, was determined. Given the true local normal area at the first static tap, the sonic ideal area, A^*, could be determined for each channel. With A^* known and, with full knowledge of the true local normal area throughout each channel, the isentropic area ratio, A/A^*, could be calculated for all locations. Then the calculation was carried out in reverse, and the Mach-area relation was used to determine Mach number, and thereafter, the isentropic ideal pressure ratio, $P/P_t|_{isen}$, at all locations within the channels.

Agreement between isentropic and experimental cases was improved by removing the approximate displacement thickness of each wall from the local normal area to define an effective, or flow usable, local normal channel area. The displacement thickness was estimated using the single parameter correlation method developed by Thwaites.[15] This final correction improved the agreement significantly, in some cases up to approximately 10% better.

Figure 16 shows the experimental-to-isentropic level of agreement for Ch #2. Agreement is very good for the lowest operating conditions, but as M_{tunnel} increases, the agreement fades. It is believed that the experimental-to-isentropic comparison should be considered a qualitative comparison at best. Since it is known that there is a flow separation within the channels from the surface oil flow visualization, it can hardly be expected that the isentropic relations used in quasi-one dimensional converging-diverging nozzle flows would be fully applicable in the highly three-dimensional, separated, internal flows found in this study. The level of agreement is best for Ch #1 and Ch #2, at small M_{tunnel}. Since the experimental data was not normalized by the true local total pressure, the difference must be attributed to total pressure losses which are known to increase with increased channel three-dimensionality (approaching the gearbox) and with velocity squared (increased M_{tunnel}).

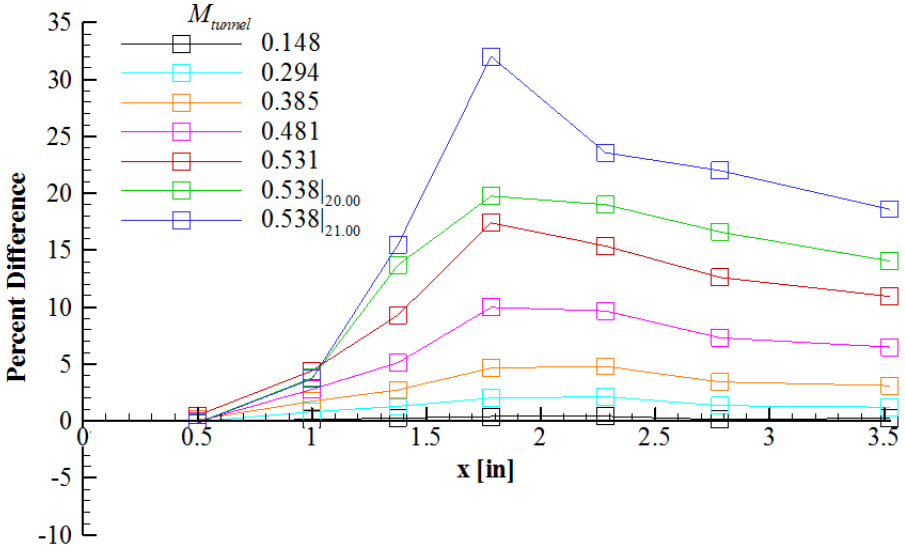

Figure 16. Percent difference between experimental and isentropic pressure ratios within Ch #2.

4. Channel Mass Flow Rate

It was previously suggested that as M_{tunnel} increases, the channels successively choke with those nearest the gearbox being the first and ending with those near θ equal zero, at which point, the entire facility chokes. In order to test this hypothesis, the mass flow rate, MFR, within each channel was calculated for increasing M_{tunnel}. To perform this calculation, local conditions at the first static pressure tap within each channel (as approximated during the experimental-to-isentropic comparison) were applied to the compressible mass flow rate formulation. Each channel's percent contribution to the total facility mass flow as a function of M_{tunnel} is displayed in Fig. 17.

The two channels nearest the gearbox fairing (Ch #4 and Ch #5) each appear to contribute equally to the total MFR and this contribution decreases minimally with increasing M_{tunnel}. The contribution that these channels provide to the total is significantly smaller than that provided by the other three channels. This may be attributed to the smaller throat local normal area found in these channels, thereby accounting to their decreased mass flow capabilities.

A clear trade-off appears to exist between Ch #3 and the two top-most channels (Ch #1 and Ch #2). As M_{tunnel} increases, the percent total mass flow passing through Ch #3 decreases, while that through the top two channels tends to increase, showing clear dumping of mass flow from Ch #3 into Ch #1 and Ch #2. The increases between the top channels are nearly identical, indicating that Ch #3 does not appear to preferentially dump into one or the other channel.

Also of interest, it was observed that for the $M_{tunnel} \leq 0.385$, the contribution to total mass flow rate did not increase with channel number in a monotonic manner. The contribution of Ch #3 fell between that of the top two channels (Ch #1 and Ch #2). This could indicate that Ch #4 and Ch #5 have trouble fulfilling their mass flow obligations even at very low M_{tunnel}, and therefore pass more mass into Ch #3.

The contribution distribution calculated in this study was compared to that calculated by Kim, Kumano, Liou, Povinelli, and Conners in Ref. 6. Comparison of operating conditions was hindered because the CFD simulation's boundary conditions were freestream values since their study encompassed the supersonic inlet as well as the bypass duct. Nevertheless, the level of agreement is quite good (Fig. 18). One area of possible contention regards the contributions of the two channels nearest the gearbox fairing. This study's results indicate that these two channels contribute equally to total MFR, whereas the CFD simulation predicts that Ch #5 contributes less than Ch #4.

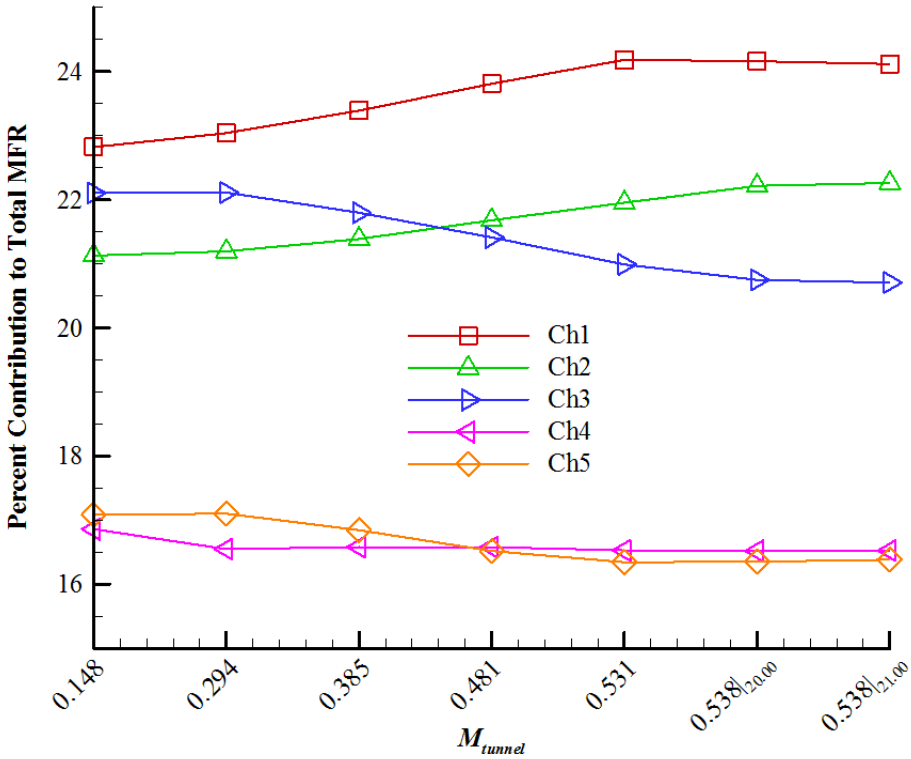

Figure 17. Channel-wise percent contribution to total mass flow rate for various prescribed experimental operating conditions.

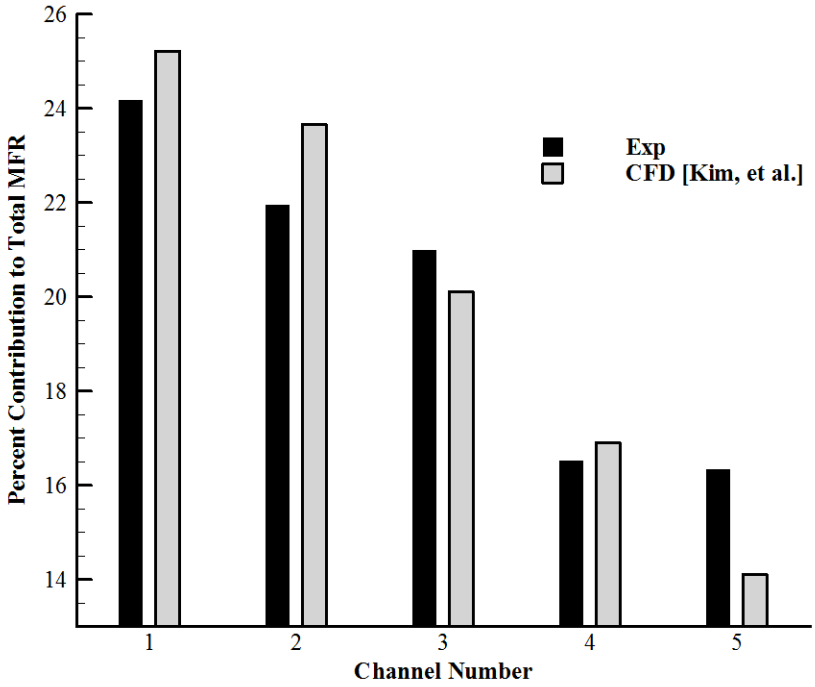

Figure 18. Comparison of the percent contribution to total mass flow rate on a per channel basis between experimental (M_{tunnel} = 0.531) and CFD study (freestream Mach number of 1.7) results.[6]

C. Flow Visualization

1. Clean Model Surface Oil Flow Visualization

Surface oil flow visualizations conducted on the clean model with both lampblack- and fluorescent-based mixtures provided insight into the flow characteristics, especially for the region behind the fairing. It was observed that flow separation occurs almost immediately after the start of the gearbox aft fairing, leading to an extremely large separation region that contains a relatively large recirculation region, (Fig. 19). The flow within the upper part of the bypass tends to carry on in the axial direction with little deviation. Both types of mixtures indicate very good symmetry between the primary and complementary sides of the model. The conclusion of this study regarding clean model performance therefore is in agreement with that of Yong[7,8] and Chiles;[9,10] without the aid of guide vanes, the aft fairing is largely ineffective and is, therefore, a source of significant pressure losses.

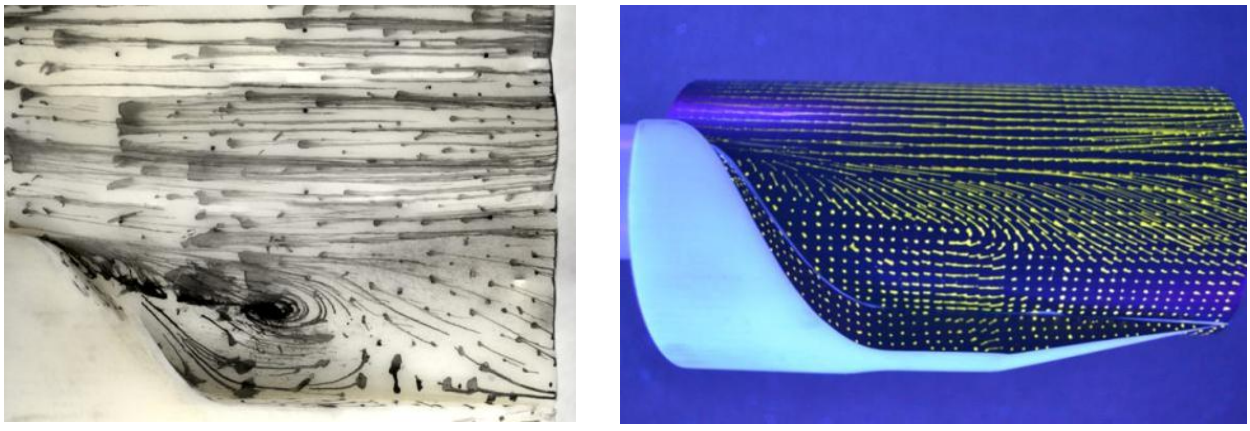

a) b)

Figure 19. Clean model surface oil flow visualization using a) lampblack-based mixture and unwrapping image, and b) the fluorescent mixture.

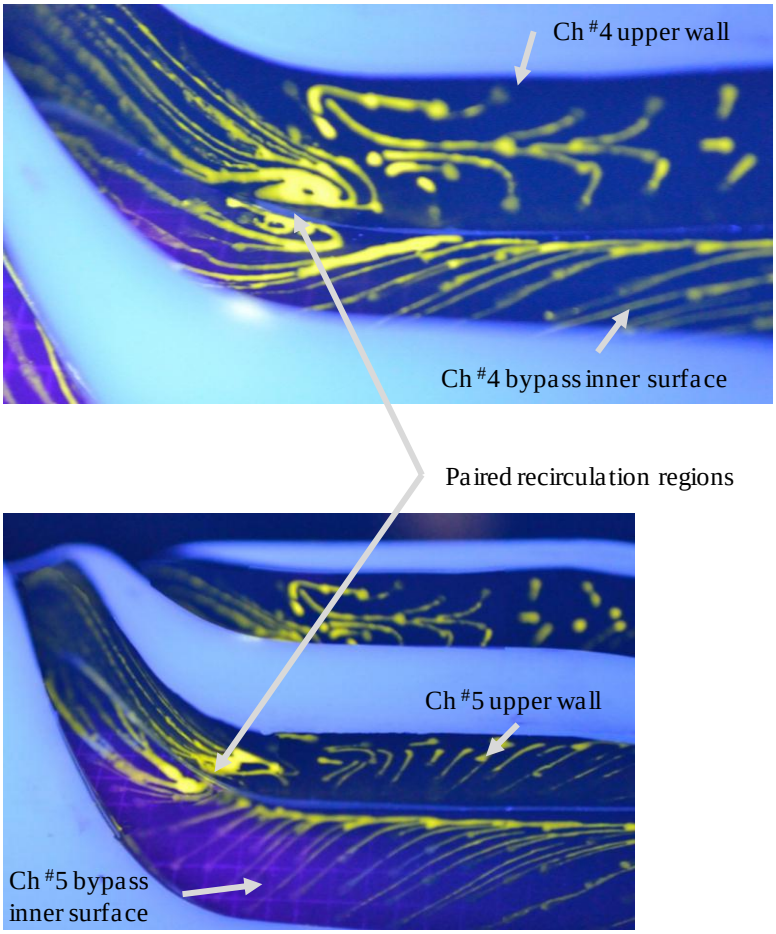

Figure 20. Vaned model channel wall characteristics for $M_{tunnel} = 0.538|_{21.00}$.

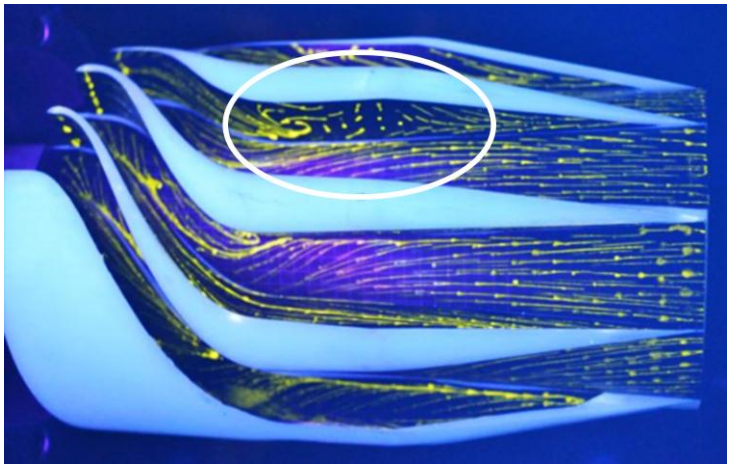

Figure 21. Vaned model fluorescent surface oil flow visualization. The circle emphasizes region of particularly interesting flow structure.

2. Additional Vaned Model Surface Oil Flow Visualization

Surface oil flow visualization of the inner surface and channel walls of the vaned aft bypass models indicate that the flow within the channels is highly complex. Very interesting and uniquely shaped recirculation regions exist on the channel walls, including paired inner bypass surface - channel wall recirculation regions (Fig. 20-21). Only Ch #1 did not display evidence of flow reversal or recirculation.

In addition to curvature, the presence of the cowling end plane seemed to also affect the channel wall surface oil flow pattern. Along several walls near x_{cowl}, (highlighted in Fig. 21), an axial stagnation point exists where some of the flow is swept downstream and is exhausted, while the rest reverses direction and moves upstream towards the recirculation regions. Vaned model surface oil flow results clearly indicate that the flow through the aft bypass model is extremely three dimensional in nature and therefore likely experiences significant pressure losses. The degree of flow complexity, qualitatively estimated by visual inspection of the oil flow results, seems to increase with increasing channel number. This observation reinforces the successive channel choking (and mass dumping) theory.

3. Schlieren Photography

Schlieren imagery with both horizontal and vertical knife edges confirm that supersonic conditions were not achieved with either model as there are no evident shocks. Both instantaneous and average images were obtained. As expected, little can be seen in the imagery of the low speed operating conditions since the density gradients were quite small. The highest operating conditions yielded interesting imagery.

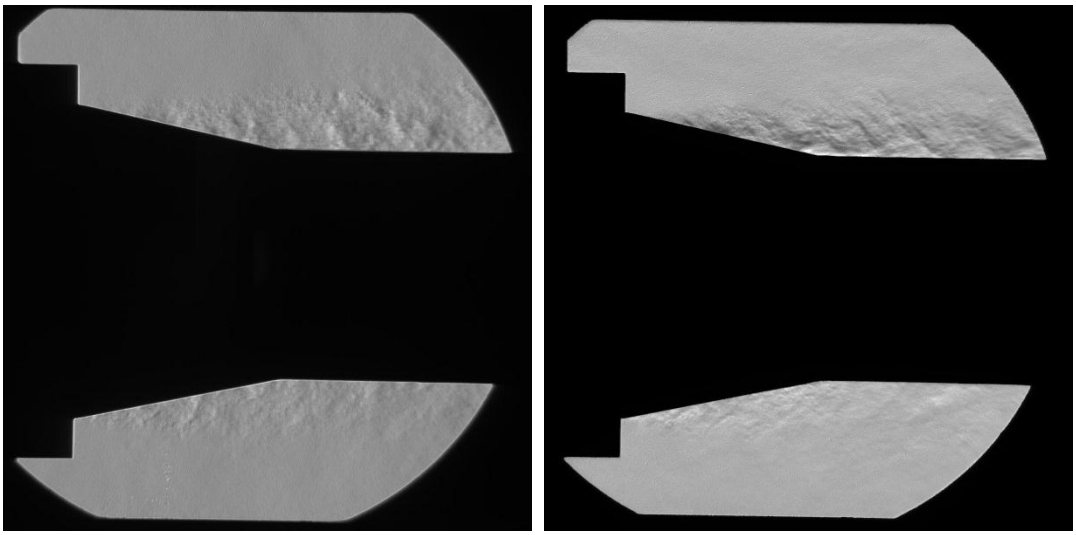

a)

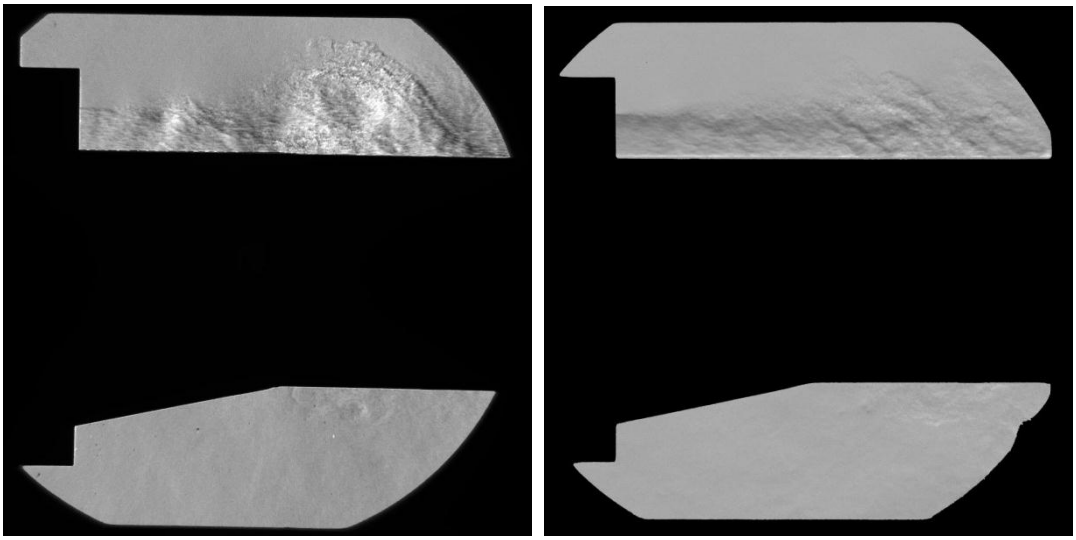

b)

Figure 22. Instantaneous Schlieren imagery with vertical (left column) and horizontal (right column) knife edges for a) the vaned model at $M_{tunnel} = 0.538|_{21.00}$ and b) the clean model at $M_{tunnel} = 0.704$.

Figure 22 presents instantaneous images of the vertical (left column) and horizontal (right column) knife edge orientations of the vaned model at $M_{tunnel} = 0.538|_{21.00}$ (top row) and the clean model at $M_{tunnel} = 0.704$ (bottom row). The vaned model does a much better job of distributing the flow around the centerbody than the clean model, as evidenced by the even feature distribution in the vaned model case (Fig. 22 a) as opposed to the highly top-favored feature distribution in the clean model (Fig. 22 b).

IV. Conclusion

A facility to evaluate the flow through the aft portion of a bypass duct with thick guide vanes was built at approximately 6% scale. Two models were used. One consisted only of the gearbox closing fairing and the second one incorporated the guide vanes. Clean model tests were conducted near the design operating condition, that is, Mach 0.700 within the fully blocked region. Vaned model tests were found to choke at Mach 0.54, well short of the design operating condition. Seven vaned model off-design operating condition tests were run, varying from Mach 0.15 to choked flow (two cases).

Normalized model surface static pressure contour plots of the clean model show that the upstream pressure ratio near the gearbox fairing walls is lower than that near the top, indicating increased Mach number near the fairing. This is consistent with the inlet plane data. The pressure ratio increases slightly with axial position, highlighted by an increase as the flow exits the cowling. Surface oil flow visualization showed that the flow separated at the onset of the fairing and that a very large recirculation region exists behind the fairing. This study supports the conclusions of previous studies regarding the relative ineffectiveness of the aft fairing sans flow guidance mechanisms.

Within the fully blocked region, inlet plane profiles indicate that total pressure is relatively uniform throughout for both model types. Mach number profiles were generated under the assumption that static pressure was uniform radially at each azimuthal station (and could therefore be measured only at the outer wall). Clean model results show a largely uniform distribution with a slightly higher core flow Mach number nearer to the gearbox fairing. Vaned model results clearly show that the flow Mach number decreases with increasing azimuthal angle as the gearbox fairing is approached. This observation leads to a successive channel choking theory, wherein it is speculated that, due to pressure losses in the channels undergoing large amounts of curvature, the mass flow rate in each channel is limited. This causes the channels nearest the gearbox to achieve choked conditions sooner than the other channels, which subsequently must pass a larger proportion of the total mass flow. In this manner, the channels successively choke with increasing facility operating condition until the last channel (nearest top-center) chokes and the facility chokes.

The normalized static pressures within each channel, plotted as a function of axial location, are similar to those associated with the quasi-one-dimensional flow within a converging-diverging nozzle. Although supersonic flow is attained, facility limitations disallowed fully supersonic flow throughout, and so shock structures can be surmised to exist within the diverging section of the channels. First static pressure tap data in each channel supports the successive choking theory.

A comparison to an isentropic ideal calculation, where experimental conditions were applied at a single location within a channel and then used to calculate ideal conditions throughout, showed good agreement for low facility operating conditions. However, increases in channel curvature or tunnel Mach number served to lessen the agreement. This suggests that the highly complex flow within the channels likely experiences large amounts of separation, contributing to total pressure losses and, thereby, the poor agreement with isentropic calculations. Surface oil flow visualization show multiple recirculation regions and other interesting flow features within the channels, which increase in number and prevalence with increasing channel curvature, further corroborating the successive choking theory.

A study of channel contribution to total mass flow rate indicates that mass dumping occurs between channels as the total mass flow increases. The two channels nearest the gearbox have relatively constant, although small, contributions to total mass flow for all operating conditions. The middle channel, however, dumps flow into the top two channels as M_{tunnel} increases. Dumping does not seem to be preferential towards one or another channel. Comparison of channel contributions to a computational study shows good agreement.

In the future, the first priority should be placed in facility modifications to allow for the collection of data at the design conditions (fully supersonic conditions). It would be very beneficial to collect total pressure data within the channels, or, at the very least, at the channel exits. This would allow for the quantification of total pressure losses within the aft bypass geometry. One key deficiency in the experimental setup as conducted in this study is that there is no core engine (hot stream) flow. Future studies might benefit from incorporating the turbofan exhaust. At the inlet plane, added azimuthal stations to provide a better annular data profile might also be beneficial, especially near the gearbox fairing.

Acknowledgments

This research was supported by Gulfstream Aerospace Corporation and Rolls-Royce plc. Any opinions, findings, and conclusions or recommendations expressed in this material are those of the authors and do not reflect the views of Rolls Royce or Gulfstream. The authors would like to thank our colleagues Tim Conners, Tom Wayman, and Robbie Cowart at Gulfstream and John Whurr at Rolls-Royce. Additionally, the authors would like to thank Greg Milner from the University of Illinois Department of Aerospace Engineering Machine Shop and Robert Coverdill of the Ford Concurrent Design and Manufacture Lab in the Department of Mechanical Science and Engineering for their assistance in facility component and test model fabrication, respectively.

References

[1]Federal Aviation Administration (FAA) Regulations. Title 14, Volume 2, Chapter 1, Section 91.817.

[2]Howe, D. C., Simmons III, F., and Freund, D., "Development of the Gulfstream Quiet Spike for Sonic Boom Minimization," AIAA 2008-0124, 2008.

[3]Cowart, R., and Grindle, T., "An Overview of the Gulfstream / NASA Quiet Spike Flight Test Program," AIAA 2008-0123, 2008.

[4]http://www.rolls-royce.com/Deutschland/en/products/tayspeydart.htm [retrieved 4 May 2011].

[5]Conners, T. R., and Howe, D. C., "Supersonic Inlet Shaping for Dramatic Reduction in Drag and Sonic Boom Strength," *44th AIAA Aerospace Sciences Meeting and Exhibit*, AIAA Paper 2006-0030, Reno, NV, Jan. 2006

[6]Kim, H. J., Kumano, T., Liou, M.-S., Povinelli, L. A., and Conners, T. R., "Flow Simulation of Supersonic Inlet with Bypass Annular Duct," *Journal of Propulsion and Power*, Vol. 27, No. 1, January-February 2011.

[7]Yeong, Y. H., Chiles, I. M., Bragg, M. B., Elliott, G. S., Loth, E., and Conners, T. R., "Wind Tunnel Testing of a Nacelle Bypass Concept for a Quiet Supersonic Aircraft," *39th AIAA Fluid Dynamics Conference*, AIAA Paper 2009-4207, San Antonio, TX, June 2009.

[8]Yeong, Y. H., "Wind Tunnel Testing of a Nacelle Bypass Concept for a Quiet Supersonic Aircraft," M.S. Thesis, Department of Aerospace Engineering, University of Illinois at Urbana-Champaign, Urbana, IL, 2009.

[9]Chiles, I. M., Loth, E., Yeong, Y. H., Bragg, M. B., and Elliott, G. S., "Computations of Engine Bypass in a Wind Tunnel Configuration," *39th AIAA Fluid Dynamics Conference*, AIAA Paper 2009-4208, San Antonio, TX, June 2009.

[10]Chiles, I. M., "Simulations of a Bypass Flow Between an Engine and a Nacelle," M.S. Thesis, Department of Aerospace Engineering, University of Illinois at Urbana-Champaign, Urbana, IL, 2009.

[11]Hererra, A. A., "An Experimental Study of the Forward Guide Vanes of an Engine Bypass Nacelle for Low-Boom Supersonic Flight," M.S. Thesis, Department of Aerospace Engineering, University of Illinois at Urbana-Champaign, Urbana, IL, 2011.

[12]Kim, H. J., Kumano, T., Liou, M.-S., and Povinelli, L. A., "Optimal Shape Design of Supersonic Bypass Inlet,", *AIAA/ISSMO Multidisciplinary Analysis Optimization Conference*, AIAA Paper 2010-9171, Fort Worth, TX, Sept. 2010.

[13]Conners, T.R., and Wayman, T.R., "The Feasibility of High-Flow Nacelle Bypass for Low Sonic-Boom Propulsion System Design," *AIAA 29th Applied Aerodynamics Conference*, AIAA Paper 2011-3797, Honolulu, HI, June 2011.

[14]Sauter, J. M., "Design of an Axisymmetric Supersonic Wind Tunnel and Experimental Study of Supersonic, Power-off Base Flow Phenomena," M.S. Thesis, Department of Mechanical Engineering, University of Illinois at Urbana-Champaign, Urbana, IL 1989.

[15]White, F. W., *Viscous Fluid Flow*, 3rd ed., McGraw-Hill, New York, NY, 2006, pp. 265-269.

[16]Jain, N., and Bodony, D. J., "Computation Assessment of Flow Through a High-Flow Nacelle Bypass," *50th AIAA Aerospace Sciences Meeting*, Nashville, TN, Jan. 2012 (submitted for publication).